

WM-97-103

September 14, 1997

# Quark-Antiquark Bound States within a Dyson-Schwinger Bethe-Salpeter Formalism

Çetin Şavkli<sup>a,1</sup>, Frank Tabakin<sup>b,2</sup>

<sup>a</sup>*Department of Physics, College of William and Mary, Williamsburg, Virginia 23185,*

<sup>b</sup>*Department of Physics & Astronomy, University of Pittsburgh, Pittsburgh,  
Pennsylvania 15260*

## Abstract

Pion and kaon observables are calculated using a Dyson-Schwinger Bethe-Salpeter formalism. It is shown that an infrared finite gluon propagator can lead to quark confinement via generation of complex mass poles in quark propagators. Observables, including electromagnetic form factors, are calculated entirely in Euclidean metric for spacelike values of bound state momentum and final results are extrapolated to the physical region.

PACS codes: 12.39.-x, 11.10St, 13.40.Gp

Keywords: quark model, bound states, confinement, mesons

---

<sup>1</sup>E-mail: csavkli@physics.wm.edu

<sup>2</sup>E-mail: frankt@tabakin.phyast.pitt.edu

# 1 Introduction

Description of simple hadrons in terms of quark-gluon degrees of freedom has long been an active area in physics. With the advent of TJNAF, which will be operating at intermediate energies and therefore probing the structure of hadrons, there is new motivation and need for a simple theoretical description of quark interactions. In this context, the Dyson-Schwinger Bethe-Salpeter(DSBS) equation formalism has gained popularity in recent years.<sup>3</sup> The DSBS formalism serves to bridge the gap between nonrelativistic quark models and more rigorous approaches, such as lattice gauge theory.

The main features of QCD can be summarized as chiral symmetry breaking, confinement and asymptotic freedom. It is possible to address all of these features within the DSBS formalism. In this formalism, the input is an effective gluon propagator which is assumed to represent the interactions between quarks at all momentum transfers. The choice of a vector interaction between quarks is motivated only by the desire to make a connection with QCD degrees of freedom. In fact, whether a scalar or a vector interaction should be used between quarks is a topic of debate not addressed in this paper.

While various applications of the DSBS formalism to pseudoscalar and vector mesons have produced promising results, there are still some questions to be investigated. In this paper, we address three issues. These are: **a)** Can an infrared gluon propagator lead to confined quarks? **b)** The question of using Euclidean metric and extrapolation. **c)** Dressing of the quark-gluon vertex in the DSBS equations while maintaining the chiral limit ?

The organization of this paper is as follows: In section 2, the model is introduced and the realization of the chiral limit, within the dressing scheme used in this paper, is discussed. In section 3, the quark propagator functions obtained by solving the Dyson-Schwinger equation are presented and the quark propagator is shown to be free of real timelike poles, indicating that quarks can not be free, which is an implication and requirement of confinement. In section 4, meson and kaon observables, which are calculated using a Euclidean metric(rather than a Wick rotation that only effects the internal momenta), are presented. Finally, results are summarized and our conclusions are presented in section

---

<sup>3</sup>See Ref. [1] for an extensive review.

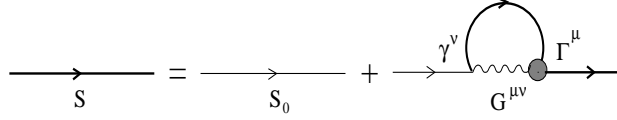


Figure 1: Quark Dyson-Schwinger equation is shown. Only one vertex is dressed to prevent double counting.

5.

## 2 THE MODEL

The mechanism of chiral symmetry breaking and recovery of massless pseudoscalar bound states(pion, kaon) in the limit of massless fermions(quarks) was originally discovered in the papers of Nambu-Jona-Lasinio(NJL) [2]. Nambu-Jona-Lasinio's model originally described relativistic nucleon interactions through local, four-nucleon couplings. It is the same philosophy that is followed in the DSBS calculations, except that now nucleons are replaced with quarks and the contact interaction is replaced by an effective gluon exchange between quarks. The Dyson-Schwinger(DS) and the Bethe-Salpeter(BS) equations employed in this work are shown in Figures 1 and 2. The DS equation describes the propagation of quarks in the presence of gluons. The BS equation describes the quark-antiquark bound state, in which the DS quark propagator is used.

In Fig. 1, the thin lines represent the current quark propagators for each flavor  $f$ :

$$i S_f^0(p) = \left[ \frac{i}{\not{p} - m_f^0} \right], \quad (1)$$

while the thick lines correspond to the dressed quark propagators:

$$i S_f(p) = \left[ \frac{i}{A_f(p) \not{p} - B_f(p)} \right]. \quad (2)$$

Here  $A_f(p)$  is a dimensionless normalization factor and  $B_f(p)$  has the units of mass(MeV).

The problem of how to systematically dress DS and BS equations has recently been addressed[3, 4]. Dressing of all vertices consistently is motivated by the desire to make a closer connection with QCD. The structure of the Dyson-Schwinger equation, when

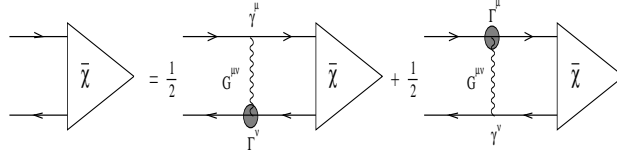


Figure 2: The Bethe-Salpeter equation is shown. Only one vertex is dressed each time. This is necessary to preserve the chiral limit, which follows from the similarity of the BS and the DS equations.

combined with the chiral limit requirement, strictly restricts the choice of kernel for the Bethe-Salpeter equation. The chiral limit in NJL type models <sup>4</sup> is obtained due to the similarity of the Dyson-Schwinger and Bethe-Salpeter equations in the limit of massless current quarks. In this limit, the quark mass function  $B(p)$  and the Bethe-Salpeter wavefunction  $\Phi(p)$  for pseudoscalar massless bound states satisfy the same equation (to be shown below). Therefore, for any given set of parameters of the model gluon propagator  $G^{\mu\nu}$ , the solution of the Dyson-Schwinger equation automatically implies a massless pseudoscalar bound state solution for the Bethe-Salpeter equation. In other words, in the chiral limit the quark Dyson-Schwinger equation produces the appropriate mass function  $B(p)$  such that the BS equation produces a massless pseudoscalar bound state.

In order to prevent double counting, only one of the vertices in the Dyson-Schwinger equation (Fig. 1) is dressed as indicated by the solid circle. Therefore, to preserve the similarity between the BS and the DS equations in the chiral limit, we dress only one of the quark-gluon vertices in constructing the BS equation. In order to keep the Bethe-Salpeter equation symmetric (to treat quarks equally), the kernel is divided into two pieces, where in each piece an alternate vertex is dressed, and contribution of those terms is averaged (See Fig. 2). While the dressing of only one of the quark-gluon vertices in the BS kernel does not represent a complete dressing, since cases where both quark-gluon vertices are simultaneously dressed are excluded, with the proper choice of vertex  $\Gamma^\mu$ , one has a *subset* of all diagrams that produce the correct chiral limit.

Having stated the general structure of the DS and BS equations used in this calcula-

---

<sup>4</sup>See Refs. [6, 7] for an extensive review of the NJL type models, and Refs. [8] for an extended version of it.

tion, we now discuss the chiral limit, and the choice of the gluon propagator  $G^{\mu\nu}(q)$ .

In terms of quark and gluon propagators, the DS equation is written as

$$S_f(p) = S_{0f}(p) + i\frac{4}{3}S_f(p)\left[\int \frac{d^4q}{(2\pi)^4} G^{\mu\nu}(p-q) \Gamma_\mu(p,q) S_f(q) \gamma_\nu\right] S_{0f}(p). \quad (3)$$

Similarly, the Bethe-Salpeter equation [9] determining the BS vertex function(a truncated wavefunction, see later)  $\chi_P(k)$  is given by

$$\begin{aligned} \bar{\chi}_P(k) = & i\frac{4}{3} \int \frac{d^4q}{(2\pi)^4} G^{\mu\nu}(q-k) \frac{1}{2} \left[ \Gamma_\nu(-k_-, -q_-) S_d(-q_-) \bar{\chi}_P(q) S_u(q_+) \gamma_\mu \right. \\ & \left. + \gamma_\nu S_d(-q_-) \bar{\chi}_P(q) S_u(q_+) \Gamma_\mu(q_+, k_+) \right], \end{aligned} \quad (4)$$

where the 4-vector  $q_+ = P\eta_1 + q$ ,  $q_- = P\eta_2 - q$ ,  $\eta_1 + \eta_2 = 1$ , and  $P$  is the bound state 4-momentum. The BS vertex function  $\chi_P(k)$  and its conjugate  $\bar{\chi}_P(k)$  are related [10] by

$$\bar{\chi}_P(ik_0, \vec{k}) = \gamma_0 \chi_P^*(-ik_0, \vec{k}) \gamma_0. \quad (5)$$

The normalization condition of the BS vertex function is derivable from the BS equation itself. [11] If the interaction does not depend on the total bound state momentum, the normalization condition reduces to

$$\begin{aligned} 2P^\mu = & iN_c \int \frac{d^4q}{(2\pi)^4} \text{tr}_D \left[ \bar{\chi}_P(q) \frac{\partial}{\partial P_\mu} S(q_+) \chi(q) S(-q_-) \right. \\ & \left. + \bar{\chi}_P(q) S(q_+) \chi(q) \frac{\partial}{\partial P_\mu} S(-q_-) \right] \end{aligned} \quad (6)$$

As it is well known, the dressing of electromagnetic vertices, such as the photon-quark vertex, is constrained by the Ward-Takahashi identity,

$$q_\mu \Gamma^\mu(p', p) = S^{-1}(p') - S^{-1}(p), \quad (7)$$

which guarantees the conservation of electromagnetic current at the vertex. Similarly, due to color current conservation, the dressed quark-gluon interaction vertex,  $\Gamma^\mu(p, q)$ , satisfies the Slavnov-Taylor identity [14]

$$q_\mu \Gamma^\mu(p', p) [1 + b(q^2)] = [1 - B(q, p)] S^{-1}(p') - S^{-1}(p) [1 - B(q, p)], \quad (8)$$

where functions  $b(q^2)$  and  $B(q, p)$  are related to “ghost fields.” Since the QCD ghost field contributions to Eq. 8 are not well understood we neglect their contributions. When ghost fields are neglected,  $b(q^2)$  and  $B(q, p) = 0$ ; the Slavnov-Taylor identity then reduces to the Ward-Takahashi identity Eq. 7. The minimal vertex that satisfies this identity in this limit has been given by Ball-Chiu [15] as:

$$\Gamma_{BC}^\mu(p', p) = \frac{A(p') + A(p)}{2} \gamma^\mu + \frac{(p' + p)^\mu}{p'^2 - p^2} \left[ \frac{A(p') - A(p)}{2} (\not{p}' + \not{p}) + B(p') - B(p) \right] \quad (9)$$

It is clear that one can add any term to this vertex that satisfies

$$q_\mu \Gamma^\mu(p', p) = 0. \quad (10)$$

Curtis-Pennington [16] have proposed such an additional vertex term. Here, for simplicity, we consider only the Ball-Chiu dressing.

## 2.1 The Chiral Limit

To determine what type of quark-gluon vertex is allowed within the approximation scheme employed here, let us analyze the chiral limit of the DS and the BS equations. In the chiral limit the current quark masses  $m_0$  and the bound state momentum  $P$  vanishes. In this limit, taking the spinor trace of the Dyson-Schwinger equation 3, one obtains

$$B(p) = \frac{i}{3} \int \frac{d^4 k}{(2\pi)^4} G_{\mu\nu}(p - k) \frac{B(k)}{A^2(k)k^2 - B^2(k)} \text{tr} \left[ \Gamma^\mu(p, k) \left( 1 + \frac{A(k)}{B(k)} \not{k} \right) \gamma^\nu \right]. \quad (11)$$

For a pseudoscalar bound state, in the chiral limit the BS vertex function is given by

$$\chi_P(k) \equiv i\gamma_5 \Phi_P(k), \quad (12)$$

where  $\Phi_P(k)$  is a scalar function of the relative momentum  $k$ , and bound state momentum  $P = 0$ . With this definition, the BS equation for the bound state wavefunction  $\Phi_P(k)$  is obtained as

$$\begin{aligned} \Phi_P(k) = & \frac{i}{3} \int \frac{d^4 q}{(2\pi)^4} G_{\mu\nu}(q - k) \frac{1}{2} \text{tr} \left[ \gamma_5 \Gamma^\nu(k, q) S_d(q) \gamma_5 \Phi_P(q) S_u(q) \gamma_\mu \right. \\ & \left. + \gamma_5 \gamma_\nu S_d(q) \gamma_5 \Phi_P(q) S_u(q) \Gamma^\mu(q, k) \right]. \end{aligned} \quad (13)$$

Commuting  $\gamma_5$  through propagators and noting that in the chiral limit,

$$S_d(-q)S_u(q) = -\frac{1}{A^2(q)q^2 - B^2(q)},$$

Eq. 13 can be rewritten as

$$\Phi_P(k) = \frac{i}{3} \int \frac{d^4 q}{(2\pi)^4} G^{\mu\nu}(q-k) \frac{\Phi_P(q)}{A^2(q)q^2 - B^2(q)} \frac{\text{tr}[(\Gamma_\mu(q,k) - \gamma_5 \Gamma_\mu(k,q) \gamma_5) \gamma_\nu]}{2} \quad (14)$$

To ensure that  $B(k)$  and  $\Phi_P(k)$  satisfy the same equation in the chiral limit, therefore producing a massless pion, the following condition should be satisfied

$$\text{tr}[\Gamma_\mu(q,k) (1 + \frac{A(k)}{B(k)} \not{k}) \gamma_\nu] = \frac{\text{tr}[(\Gamma_\mu(q,k) + \Gamma_\mu(k,q)) \gamma_\nu]}{2} \quad (15)$$

Clearly, the commonly used bare quark gluon vertex,  $\Gamma_\mu = \gamma_\mu$  satisfies this condition. Furthermore, the condition Eq. 15 is also satisfied by the following part of the Ball-Chiu vertex

$$\Gamma^\mu(p', p) = \frac{A(p') + A(p)}{2} \gamma^\mu + \frac{(p' + p)^\mu}{p'^2 - p^2} \frac{A(p') - A(p)}{2} (\not{p}' + \not{p}). \quad (16)$$

The  $B(p') - B(p)$  part of the Ball-Chiu vertex would have contributed to the lefthandside of Eq. 15 while it does not contribute to the righthandside. The contribution of this term is small compared to the sum of other two terms. Therefore, it is a good approximation to drop this term. The vertex Eq. 16 enables us to preserve the chiral limit while including the dominant part of the quark-gluon vertex dressing as suggested by the Ward-Takahashi identity. This approximate form(Eq. 16) of the Ball-Chiu vertex is used for the *quark-gluon coupling* in this work.

Since the functions  $B(k)$  and  $\Phi_P(k)$  satisfy the same equation in the chiral limit, they are equal upto a proportionality constant. With the help of the BS normalization condition 6 it is found [12, 13] that

$$\Phi_P(k) = \frac{1}{f_\pi} B(k), \quad (17)$$

where  $f_\pi$  is the pion decay constant.

In order to complete the description of the model, one needs to choose a model for the gluon propagator  $G^{\mu\nu}(q)$ . The choice of  $G^{\mu\nu}(q)$  has been discussed in various papers[17].

Usually, the ultraviolet( $q \rightarrow \infty$ ) or asymptotic behavior of  $G^{\mu\nu}(q)$  is borrowed from QCD calculations, while its infrared( $q \rightarrow 0$ ) or confining behavior is given by a sharply falling function such as  $1/q^4$  or  $\delta^4(q)$ , to incorporate confinement. The problem with  $1/q^4$  behavior is that it is not an integrable singularity and one needs to introduce an infrared cutoff. While the  $\delta^4(q)$  form does not have this problem, it is perhaps too simple a form to represent the physics in the infrared region; this issue requires further study. **In this paper, we show that an infrared finite propagator can not be ruled out on the basis of quark Dyson-Schwinger and Bethe-Salpeter equations.** The model used here is

$$G^{\mu\nu}(q) = (g^{\mu\nu} - \frac{q^\mu q^\nu}{q^2}) [G_{\text{IR}} + G_{\text{UV}}], \quad (18)$$

where the infrared( $q \rightarrow 0$ ) behavior,  $G_{\text{IR}}$ , is modeled by a finite term

$$G_{\text{IR}}(q) = G e^{-q^2/\sigma^2}, \quad (19)$$

while the asymptotic( $q \rightarrow \infty$ ) form,  $G_{\text{UV}}$ , is taken from perturbative QCD calculations

$$G_{\text{UV}}(q) = 2\pi^2 \frac{d}{(q^2 + \sigma^2) \ln(\tau + q^2/\Lambda_{QCD}^2)}, \quad (20)$$

with  $d = 12/(33 - 2N_f) = \frac{4}{9}$ , where  $N_f = 3$  is the number of flavors. The QCD scale parameter  $\Lambda_{QCD}$ , determined by fitting high energy experiments(Particle Data Group, 1990), is chosen to be 225 MeV. The constant  $\tau$  ensures the positivity of the asymptotic piece as  $q \rightarrow 0$ , and results are not very sensitive to this parameter. The  $\tau$  is chosen to be  $\tau = 3$ . The  $\sigma^2$  in the denominator of the UV piece is introduced to ensure that the infrared piece is the dominant contribution at low energies. Similar forms for the dressed gluon propagator have been used in the literature[18, 19, 20, 21] with considerable success in preliminary applications of Dyson-Schwinger Equations to hadronic physics. Here, we develop this approach using a dressed quark-gluon vertex while maintaining the chiral limit, **and show that quarks can be confined with an infrared finite interaction.** Aside from current quark masses,  $m_{u,d} \approx 6 \pm 2$  MeV and  $m_s \approx 150 \pm 50$  MeV [22], which are also the input parameters of QCD, there are only **two** unconstrained parameters( $G, \sigma$ ) to vary to predict the data. Parameters  $G = 1.9710^{-4} \text{MeV}^{-2}$  and  $\sigma = 750$  MeV are chosen to give the optimum overall fit. We choose the current quark mass of the strange quark to



fine tune the kaon mass. The current quark masses used in the calculation are:  $m_{u,d} = 3$  MeV, and  $m_s = 60$  MeV. The ratio  $m_s/m_u$  is well within acceptable limits [22]. In the next section, we discuss the solution of the quark Dyson-Schwinger equation.

### 3 QUARK PROPAGATORS AND CONFINEMENT

The numerical solution of the DS equation Eq. 3 is performed through iteration to find the quark propagator functions  $A(p^2)$  and  $B(p^2)$  in Euclidean metric. The details of the numerical methods are explained in the Appendix. Solutions for  $A(p^2)$  and  $M(p^2) \equiv$

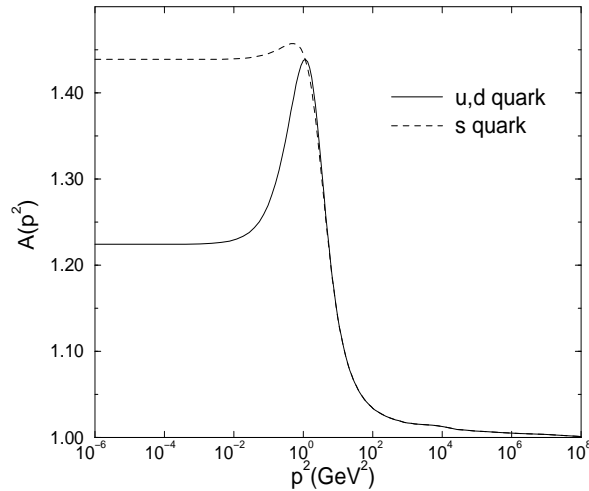


Figure 3: The quark propagator function  $A(p)$  is shown for up/down, and strange quarks. Dressing of the quark-gluon vertex causes the peak observed in  $A(p)$ .

$B(p^2)/A(p^2)$  in the spacelike region are shown in Figures 3 and 4. According to the results in Figures 3 and 4, for low momenta ( $p < 1$  GeV) quark masses are close to those of the constituent quarks; whereas, as momentum increases, quarks start behaving as current quarks ( $A_f(q^2) \rightarrow 1, B_f(q^2) \rightarrow m_0$ ). In the infrared region, the quark masses approach the constituent mass values. The behavior of function  $A_f(q^2)$  is different than that of  $M_f(p^2)$ ;  $A_f(q^2)$  reaches its maximum value at intermediate energies, where the scale is given by  $\sigma$ . This is a different behavior than results presented in Ref. [17], for the bare

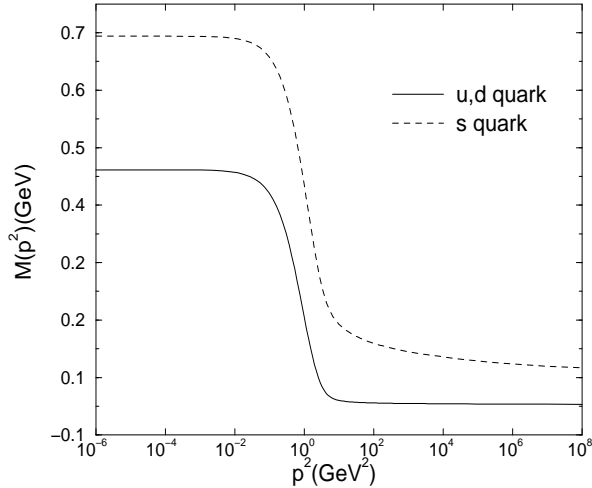


Figure 4: Quark mass functions  $M(p)$  are shown for up/down, and strange quarks. At the origin( $p^2 = 0$ ), quark masses are closer to constituent quark mass values used in nonrelativistic quark models. Asymptotically, quark mass values approach current quark mass values.

quark-gluon coupling case. In their results, both  $M(p^2)$  and  $A_f(q^2)$  are monotonically decreasing functions. In our case, the dressing of the quark-gluon vertex gives rise to the nonmonotonic behavior we found for  $A_f(q^2)$ . As one increases the coupling strength  $G$ , monotonic behavior of  $A$  is restored.

### 3.1 Test of Confinement

Confinement is the property that only color singlet hadrons are observed in nature. In QCD, confinement is obtained dynamically due to the nonabelian, hence self-interacting, nature of gluons. A natural result of confinement is that no free quark state should be observed(a free quark state has a net color.) In QFT, an *n-body bound state* is defined by the pole of the n-body propagator. The familiar 2-body(Bethe-Salpeter, Gross) and 3-body(Faddeev) equations are obtained, based on this definition, by looking for the poles in the two and three body propagators. Similarly, it is natural to expect that a 1-body(or *free*) state should be identified by the pole of the one body propagator. Therefore, if

quarks are confined, quark propagators should not have poles in the timelike( $p^2 > 0$ ) region.<sup>5</sup>, because such a pole permits an asymptotically(in space) free quark wave to exist. The absence of poles in the quark propagators is, however, not conclusive evidence for confinement. In order to be able to claim that a theory is confining, one has to also show that a diquark, or any other color nonsinglet stable bound state does not exist. Here, we restrict our discussion of confinement to quarks only. Therefore from here on, “confinement” refers to “lack of free quarks” rather than the more general definition of “lack of colored states.” In order to test whether a quark propagator, given in Euclidean metric, leads to confinement, one needs a procedure to determine the presence of any poles in the timelike region.<sup>6</sup> For simple cases such as a free fermion, the Euclidean expression for the propagator can be readily used to see if there are any poles when the propagator is continued to the Minkowski metric, i.e.

$$\frac{1}{p_E^2 + m^2} \rightarrow \frac{1}{p^2 - m^2}, \quad (21)$$

where there is a pole at  $p^2 = m^2$ . For the dressed quark propagator, the confinement test question is: does

$$\frac{B(p_E^2)}{A^2(p_E^2)p_E^2 + B^2(p_E^2)} \quad (22)$$

have a pole? For this test, the procedure used in Ref. [25] is adopted to determine whether a quark propagator given in Euclidean metric has poles, when continued to Minkowski metric. The starting point is the definition of a generalized quark propagator

$$S(p) \equiv \int d\mu \rho(\mu) \frac{i}{\not{p} - \mu}, \quad (23)$$

where  $\rho(\mu)$  is a spectral density function. The Euclidean metric expression for  $\text{tr}[S_E(p)]$  is

$$\text{tr}[S_E(p)] = 4 \int d\mu \rho(\mu) \frac{\mu}{p^2 + \mu^2}. \quad (24)$$

---

<sup>5</sup>There is an alternative to this approach, which is developed within the context of the Gross equation in Ref. [23]. In that approach, quarks are allowed to be on shell as long as they are in the vicinity of off-shell quarks, and confinement is realized through a relativistic generalization of the linear potential.

<sup>6</sup>An alternative realization of confinement can be obtained by simply defining the quark mass function such that quark can never be on shell.[5] This approach amounts to having quark mass function  $M(p^2)$  as input and the effective gluon propagator  $G^{\mu\nu}(q)$  as unknown in the quark Dyson-Schwinger equation. In this approach, a unique determination of the gluon propagator is not possible. Therefore, one is forced to make a separable interaction approximation.

Using contour integration methods, the Fourier transform of this trace is found to be

$$\Delta(t) = \int \frac{dp}{2\pi} e^{ipt} \text{tr}[S_E(p)] \quad (25)$$

$$= 2 \int d\mu \rho(\mu) e^{-\mu t} . \quad (26)$$

We define  $\bar{\mu}(t)$ , the average effective mass(pole location) of the propagator  $S(p)$  as a function of time by

$$\bar{\mu}(t) \equiv -\frac{\partial}{\partial t} \ln(\Delta(t)) \quad (27)$$

$$= \frac{\int d\mu \rho(\mu) \mu e^{-\mu t}}{\int d\mu \rho(\mu) e^{-\mu t}} . \quad (28)$$

Let us assume that  $S(p)$  has at least one pole for a finite  $p^2 > 0$ . Let  $\rho(\mu) = \sum_{i=0}^{n-1} c_i \delta(\mu - m_i)$ , where  $n \geq 1$  and  $m_i < m_{i+1}$ . This assumption leads to a discrete average

$$\bar{\mu}(t) = \frac{\sum_{i=0}^{n-1} c_i m_i e^{-m_i t}}{\sum_{i=0}^{n-1} c_i e^{-m_i t}} . \quad (29)$$

Taking the limit of this expression at infinite time  $t \rightarrow \infty$ , one has

$$\lim_{t \rightarrow \infty} \bar{\mu}(t) \cong m_0. \quad (30)$$

Therefore, this averaging procedure gives the smallest pole of the propagator  $S(p)$ . If this limit exists and it is real, then there is at least one finite pole for timelike momenta in the Minkowski metric, and therefore the propagator does not represent a spatially confined particle. On the other hand, if there is no finite limit or the limit is complex, then the propagator represents a confined particle, since the propagator does not have a real finite pole. This test for confinement has been applied to the quark propagator obtained from the numerical solution of the Dyson-Schwinger equation. There are three possible pole structures for the quark propagator. These possibilities are exemplified by the following:

- Real pole:

$$\begin{aligned} S_E(p_E) &= \frac{1}{p_E^2 + m^2}, \\ \Delta(t) &\propto e^{-mt}, \\ \bar{\mu}(t) &= m, \end{aligned}$$

where the test produces the pole location as expected.

- Absence of poles:

$$\begin{aligned} S_E(p_E) &= e^{-p_E^2/(2\sigma^2)}, \\ \Delta(t) &\propto e^{-\sigma^2 t^2/2}, \\ \bar{\mu}(t) &= \sigma t \rightarrow \infty, \end{aligned}$$

In this example, there is no finite pole and the propagator represents a confined particle. This analytic form is the same as the infrared piece of the effective gluon propagator 19.

- Complex poles:

$$S_E(p_E) = \frac{1}{(p_E - ia)^2 - m^2},$$

Here the pole is complex in general and purely imaginary when  $a = 0$ . For this case, the test results gives analytically

$$\begin{aligned} \Delta(t) &\propto e^{-at} \sin(mt), \\ \bar{\mu}(t) &= a + m \tan(mt - \frac{\pi}{2}). \end{aligned}$$

Therefore, the signature of complex poles appears as  $M(t) \equiv \bar{\mu}(t) \propto \tan(mt)$  behavior as  $t \rightarrow \infty$ , where the frequency of oscillations is proportional to the imaginary part of the quark mass pole. This is exactly the type of behavior found by applying the confinement test to the quark propagator obtained by numerically solving the DS equation 3. Since the quark propagator is known only numerically, application of the test is numerical and details of the numerical methods are explained in the Appendix. Here we present the test results for three different coupling strengths, namely  $G = 1 \times 10^{-4}, 1.5 \times 10^{-4}$ , and  $1.97 \times 10^{-4} \text{MeV}^{-2}$ . The first case,  $G = 1 \times 10^{-4} \text{MeV}^{-2}$  is shown in Figure 5. According to this result, the pole location is finite ( $\approx 110 \text{MeV}$ ) and real. Therefore, this quark propagator does not represent a confined particle. On the other hand, this is a case where the coupling constant is very small. As one increases the strength of the coupling to  $G = 1.5 \times 10^{-4} \text{MeV}^{-2}$  an irregular oscillatory behavior sets in (Fig. 6). If the coupling strength is further increased to  $G = 1.97 \times 10^{-4} \text{MeV}^{-2}$ , which is the parameter that is used to fit all observables in this paper, **the oscillations clearly displays the**

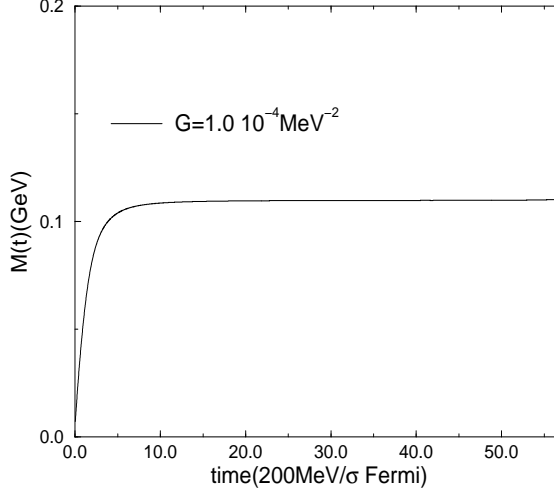


Figure 5: Mass pole as a function of time is shown. Asymptotically,  $M(t)$  approaches a constant, which indicates a real mass pole(unconfined quark).

$\tan(mt)$  behavior(Fig. 7) which indicates that quarks have complex mass poles. According to this result(Fig. 7), the average distance a quark can travel before it hadronizes, which is given by the average distance between the peaks(singularities) of the  $M(t)$  function, is approximately  $D \times 200\text{MeV}/\sigma \text{ Fermi} = 1.45 \times 200/750 = \mathbf{0.39 \text{ Fermi}}$ , where  $D \approx 1.45$  is the average spacing between the peaks. This result is in very good agreement when compared with the sizes of various hadronic bound states such as the pion( $r_\pi = .66 \text{ Fermi}$ ) and the kaon( $r_K = .53 \text{ Fermi}$ ). A recent study [24] of the DS equation within the context of QED in three dimensions similarly finds complex conjugate mass poles in the fermion propagator. It is important to emphasize that the analytic form of the gluon propagator used in this calculation is not the only possible choice to produce confined quarks. In fact, we have obtained similar results with other infrared singular gluon propagators. Therefore, it is not possible to single out a specific analytic form for the gluon propagator solely on the basis of the confinement test. Just as there are infinitely many confining potentials in nonrelativistic quantum mechanics, there are infinitely many confining effective gluon propagators in field theory. Therefore, additional

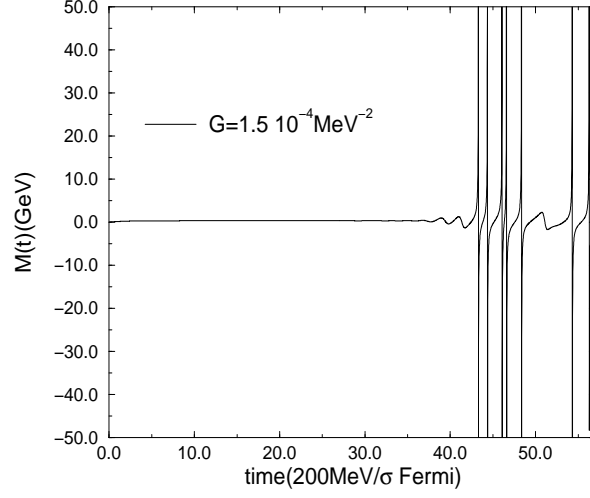


Figure 6: Mass pole as a function of time is shown. Oscillations indicate that quark mass pole is complex.

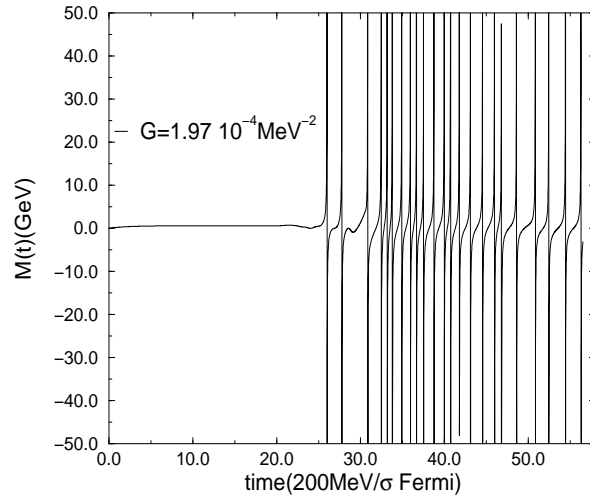


Figure 7: As the strength of the coupling,  $G$ , is increased  $M(t) \propto \tan(t)$  behavior clearly sets in.

tests such as the prediction of meson observables are needed to determine if the gluon propagator ansatz makes physical sense.

Having shown that it is possible to obtain confined quarks using a gluon propagator with a gaussian type of infrared behavior, we now turn to the quark-antiquark bound state problem.

## 4 QUARK-ANTIQUARK BOUND STATES

Before we embark on solving the BS equation, it is necessary to clarify a technical problem. In the previous section, dressed quark propagators were calculated in the Euclidean metric(or spacelike momentum region). For the Bethe-Salpeter equation, usage of the Euclidean metric is more problematic.<sup>7</sup> Unlike the quark Dyson-Schwinger equation, the Bethe-Salpeter equation involves the external total bound state momentum  $P$ , which has to eventually represent a physical particle(bound state) with a real positive mass. Therefore, the four momentum of the particle should be  $P = (m, \vec{0})$ , for which  $P^2 = m^2 > 0$  represents a timelike particle. It follows that, in order to be able to perform the integrations in Eq. 4 in Euclidean metric, one needs to know the functions  $A(q_+^2), B(q_+^2)$  for  $q_+^2 = m^2\eta_1\eta_2 - q^2 + i m q_0$ , where  $\eta_{1,2}$  is chosen to be

$$\eta_{1,2} = \frac{m_{1,2}}{m_1 + m_2}, \quad (31)$$

and  $m_{1,2} \equiv M_{u,d}(0)$ . On the other hand, functions  $A(q_+^2), B(q_+^2)$  are known only for real and spacelike  $q_+^2$ . The thick line in Fig. 8(the positive  $q_+^2$  axis) is where functions  $A(q^2)$  and  $B(q^2)$  has been calculated by solving the Dyson-Schwinger equation. The domain where these functions are needed is shown by the shaded region in Fig. 8. At this point, there are three options. The first one, used in Ref. [28] among other works, is to assume an analytic functional form that fits the numerical functions  $A(q^2), B(q^2)$  on the positive real axis. Once this assumption is made one can use these analytic functions over the entire complex plane. The second approach, which has been used in Ref. [18], is to Taylor expand the functions  $A(q^2), B(q^2)$  around their real values to extend the results to the complex plane. Both of these methods have drawbacks. It has been shown in previous

---

<sup>7</sup>Recent efforts to solve the BS equation directly in Minkowski metric are given in Refs. [26, 27]



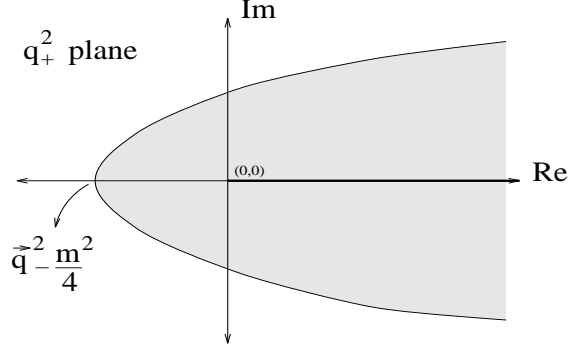


Figure 8: Argument domain of functions  $A(q_+^2)$  and  $B(q_+^2)$  for physical bound states ( $m^2 > 0$ ). The positive axis shows the spacelike  $q_+^2$  region.

section that the quark propagator has complex conjugate mass poles in the spacelike region. It has also been shown[29] that functions  $A(q^2), B(q^2)$  possibly have poles and branch cuts in the complex plane, which complicates the above methods. Therefore sampling the momentum values away from the spacelike momentum axis is problematic. We follow a third approach, which is also used in lattice gauge theory calculations. In this approach, the bound state problem is solved for a set of spacelike bound state momenta,  $P^2 = -m^2 < 0$ , which transforms the problem to Euclidean metric, thereby avoiding the complex argument problem, and the final results are then extrapolated back to the physical region,  $P^2 > 0$ . Since it is the final results such as form factors and decay constants that are extrapolated (rather than functions  $A(q^2), B(q^2)$ , which are integrated out in calculations of observables), this method has the benefit of explicitly displaying the reliability of the extrapolation. The only assumption is the analyticity of the *observables* as a function of the bound state mass. **In this method, there is no need to assume that functions  $A(q^2), B(q^2)$  are analytic.** The procedure for the solution is as follows: First the Bethe-Salpeter equation 4 is discretized<sup>8</sup> and transformed into a matrix Equation

$$H_{P^2} \Phi = \Phi, \quad (32)$$

where  $P^2 = m^2 > 0$  is the bound state mass and the implicit eigenvalue of this matrix equation. Since Eq. 32 will be solved for spacelike bound states  $P^2 = m_i^2 < 0$ , one will

---

<sup>8</sup>see Appendix for details of our numerical techniques.

not be able to find any solutions unless an artificial eigenvalue  $\alpha_i$  is introduced to Eq. 32

$$H_{m_i^2} \Phi = \alpha_i \Phi. \quad (33)$$

One proceeds by finding a set of solutions  $\{m_i^2 < 0, \alpha_i\}$  to the above equation. This is done by using an inverse iteration technique as explained in the Appendix. Using the set of solutions  $\{m_i^2 < 0, \alpha_i\}$ , a functional relationship between  $\alpha_i$  and  $m_i^2$  can be established

$$\alpha_i = f(m_i^2). \quad (34)$$

It is only when  $m_i^2 = m^2 > 0$  and  $\alpha_i = 1$  that one recovers the original BS equation(32). Therefore, location of the  $m^2$  that gives  $\alpha = 1$  is the eigenvalue and mass of the physical bound state in question. The most general form for the spin-space part of the BS vertex function for pseudoscalar mesons is given by

$$\chi_P(k) = i\gamma_5[\Phi_0 + \not{P} \Phi_1 + \not{k} \Phi_2 + [\not{k}, \not{P}] \Phi_3]. \quad (35)$$

In the pseudoscalar meson channel, the dominant contribution to the BS vertex function comes from the first term [18, 19],

$$\chi_P(k) \approx i\gamma_5 \Phi_P(k) \quad (36)$$

This dominance is not surprising since the Dirac structure of the leading term in 36 is the same as that of pointlike pion-quark coupling. Therefore, we only consider the leading term in our analysis.<sup>9</sup> The angular dependence of the BS vertex function is made explicit by expanding it in terms of Tchebyshev polynomials

$$\Phi_P(k) = \sum_{n=0}^{\infty} \Phi_P^n(|k|) T^n(\cos\gamma). \quad (37)$$

For the bound states considered in this work( $\pi, \pi^*, K^\pm$ ), the dominant contribution to  $\Phi_P(k)$  comes from the  $T_0$  polynomial. Test runs for cases where higher( $n > 0$ ) Tchebyshev polynomials are included showed that the contribution of the higher Tchebyshev polynomials are negligible, which is in agreement with conclusions in Ref. [18]. After

---

<sup>9</sup>For vector mesons, the leading term might not be the only important one.

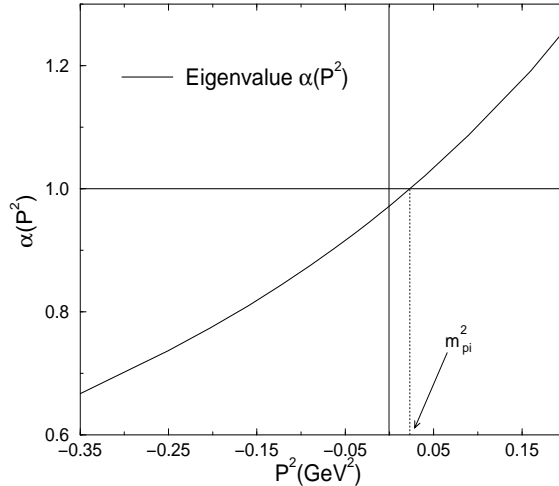


Figure 9: Dependence of eigenvalue  $\alpha$  on  $P^2 = m_\pi^2$ . Location of the bound state momentum is given by the intersection defined by  $\alpha = 1 = f(P^2)$ .

solving the BS equation numerically, a relationship 34 between the largest eigenvalue<sup>10</sup>  $\alpha$  and  $m^2$  is constructed by using a polynomial fit

$$\alpha = \sum_{i=0}^n c_i (m^2)^i. \quad (38)$$

It has been determined that for all of the bound states under consideration  $n = 3$  gave a satisfactory fit. The extrapolations done to find the pion and kaon masses are shown respectively in Fig. 9 and Fig. 10. The pion ground and first excited state and kaon groundstate wavefunctions are shown in Fig. 11. The first excited state of the pion has a node, while the ground state wavefunctions are positive definite. The kaon BS wavefunction is more spread out in momentum space than that of pion.

## 4.1 The Electromagnetic form factor using Euclidean metric

Electromagnetic current conservation

$$\partial_\mu J_{em}^\mu = 0, \quad (39)$$

---

<sup>10</sup>The second largest  $\alpha$  leads to the first excited state.

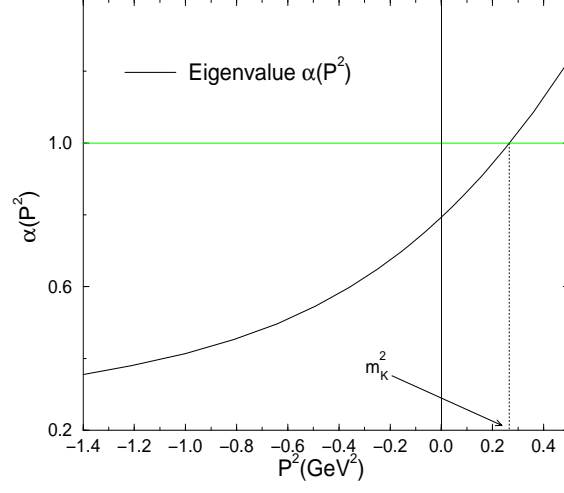


Figure 10: Determination of kaon mass.

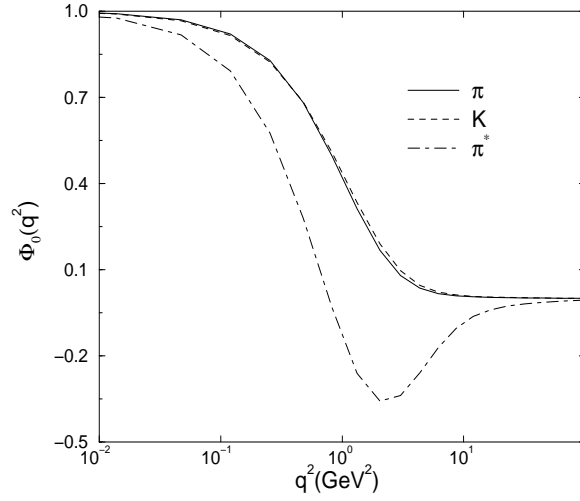


Figure 11: The pion and kaon ground and pion first excited state BS wavefunctions  $\Phi_P^0(|k|)$  are shown all for  $P^2 = 0$ .

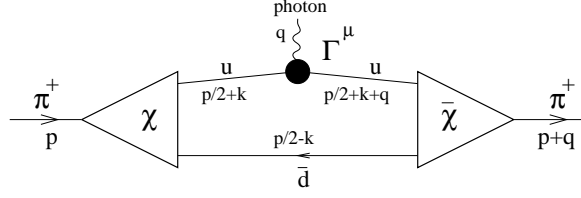


Figure 12: Electromagnetic Form Factor of Pion in the impulse approximation(i.e. interaction of the initial and final pion with each other is neglected.)

implies that in momentum space one must have  $q_\mu J_{em}^\mu = 0$ . Since both initial and final pion states are on their mass shells, we have  $p^2 = m^2 = (p+q)^2$ , or  $2p \cdot q + q^2 = 0$ . Therefore, the definition of the form factor takes the following form

$$\langle \pi^+(p+q) | J_{em}^\mu(0) | \pi^+(p) \rangle = F_\pi(q^2)(2p^\mu + q^\mu). \quad (40)$$

This matrix element is represented by the Feynman diagram shown in Figure 12.<sup>11</sup> As the photon momentum  $q$  vanishes, the pion is perceived as a point charge. Therefore, it is expected that  $F(0) = e$ , and the charged pion has an electromagnetic charge of  $e$ . To arrive at this result, two conditions must be satisfied; namely, the BS wavefunction should be properly normalized, and the conservation of the electromagnetic current at the photon-quark interaction vertex should be taken into account. The dressed electromagnetic vertex function  $\Gamma^\mu(p', p)$  for the photon quark coupling satisfies the Ward-Takahashi identity Eq. 7, which is an indirect statement of the conservation of the electromagnetic current. For the *photon-quark* vertex we use the full Ball-Chiu vertex 9. In the Breit frame, the initial and final pion momenta are

$$P_i = (i\sqrt{m_i^2 - \frac{q^2}{4}}, 0, -\frac{q}{2}), \quad P_f = (i\sqrt{m_i^2 - \frac{q^2}{4}}, 0, \frac{q}{2}). \quad (41)$$

Therefore,  $(P_i)^2 = (P_f)^2 = -m_i^2 < 0$  are both spacelike. Calculation of the form factor is done for a set of spacelike bound state masses  $m_i^2$ , ( $i = 1 \cdots 21$ ) and the resultant set of form factor functions are extrapolated at each photon momentum. For example, the pion

<sup>11</sup>Only the interaction of the photon with the u quark is shown. There is also a second diagram where the photon interacts with the  $\bar{d}$  quark.

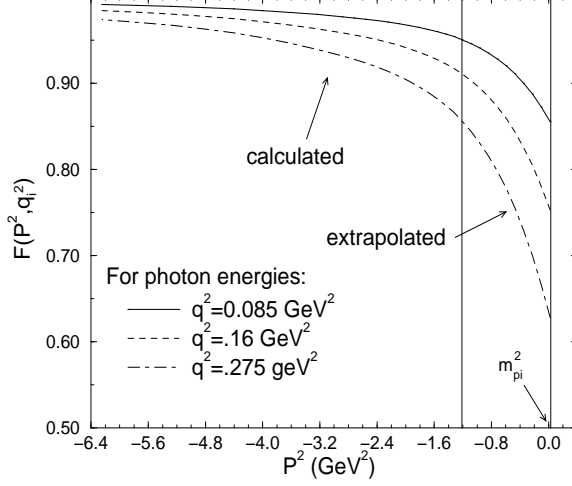


Figure 13: These plots show how the form factor extrapolation is done for various photon energies. The extrapolated results are on the right hand side (timelike,  $P^2 = m_\pi^2 > 0$ ) of bound state momentum axis.

form factor at photon momentum of  $q_i^2$  is

$$F(m^2, q_i^2) = \sum_{j=0}^n C^j(q_i^2) m^{2j}, \quad (42)$$

where  $C^j(q_i^2)$  are the coefficients of a fit to the numerical result for  $F$  for photon momentum of  $q_i^2$ . Therefore, the physical result for the pion form factor at the photon momentum  $q_i^2$  is  $F(M_\pi^2, q_i^2)$ . In Figure 13, we show the extrapolation for three different photon momenta,  $q^2 = 0.085 \text{ GeV}^2$ ,  $q^2 = 0.16 \text{ GeV}^2$ , and  $q^2 = 0.275 \text{ GeV}^2$ . For each case, the result of extrapolation is given by the value of the form factor functions at  $P^2 = m_\pi^2$ . In order to ensure the reliability of the fit, a large number(21) of form factor calculations *at each photon momentum* has been performed. The order of the polynomial fit used is  $n = 7$ . According to the extrapolation results(Fig. 13) as the photon momentum increases, the reliability of the extrapolation decreases. This difficulty is common to all solution methods(within the covariant DS-BS formalism) which use Euclidean metric.<sup>12</sup> The reason for

<sup>12</sup>See Refs. [32] for a discussion of the transition to asymptotic(large  $q^2$ ) behavior of the pion form factor within a light-cone Bethe-Salpeter formalism.

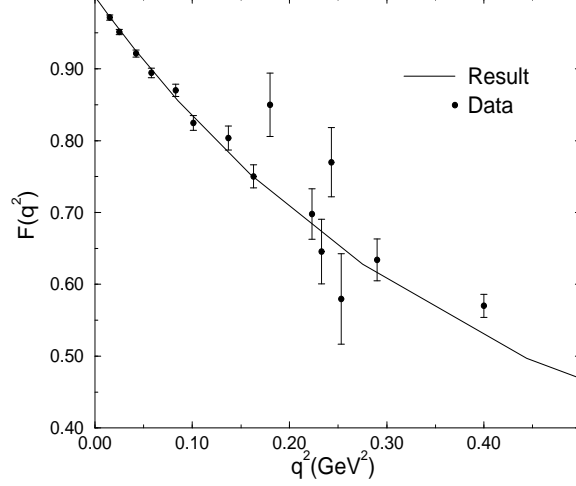


Figure 14: Extrapolated result for electromagnetic pion form factor.

this sensitivity is the increase in the curvature of the function  $F(m^2, q_i^2)$  with increasing  $q_i^2$ . We present the form factor calculation for pion(Fig. 14) and kaon(Fig. 15) cases in the region where the extrapolation is reliable. The data points for the pion form factor are taken from Refs. [33, 34]. Data available from earlier experiments [35, 36] for the kaon form factor are very poor. Experiments at TJNAF will hopefully provide better measurements for both pion and kaon form factors. The pion decay constant,  $f_\pi$ , is defined by the vacuum to one pion matrix element of the axial vector current:

$$\langle 0 | J_{5\mu}^i(x) | \pi^j(p) \rangle \equiv i f_\pi \delta^{ij} p_\mu e^{-ip \cdot x}. \quad (43)$$

For a  $\pi^+$  meson at  $x = 0$ , this definition becomes:

$$\langle 0 | \bar{\Psi}_d(0) \gamma_\mu \gamma_5 \frac{\lambda^-}{2} \Psi_u(0) | \pi^+(p) \rangle \equiv i f_\pi p_\mu. \quad (44)$$

This matrix element corresponds to the Feynman diagram shown in Figure 16. Calculation of decay constants are done using the same type of extrapolation technique used in the calculations of masses and form factors. Values found are  $f_K = 90.3(113)$  MeV, and  $f_\pi = 77.2(92.4)$  MeV, where numbers in parenthesis are the experimental measurements. The

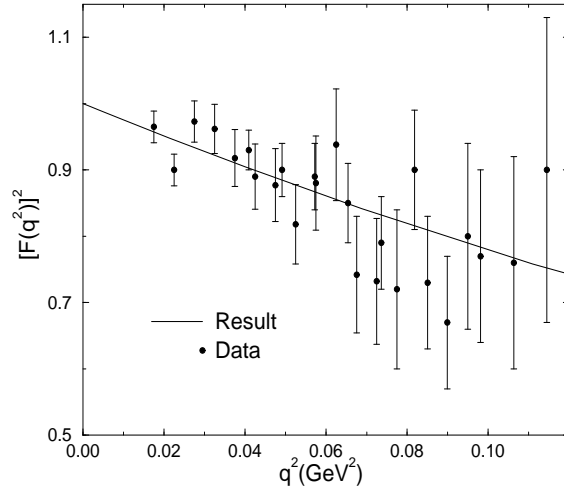


Figure 15: Electromagnetic form factor of Kaon.

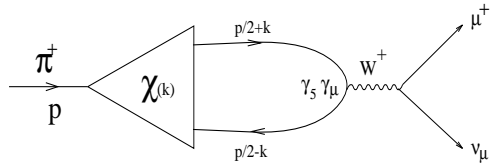


Figure 16: Pion Decay



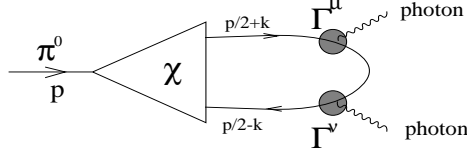


Figure 17: Neutral Pion Decay.

ratio of decay constants  $f_K/f_\pi = 1.17(1.22)$  is in good agreement with the experimental value and comparable to those found in similar works. It is reported in Ref. [20] that next to leading order terms of the vertex function 35 contribute significantly to the decay constants. This is a possible explanation for the low values we find for the decay constants.

As a final application, the neutral pion decay to two photons,  $\pi \rightarrow \gamma + \gamma$  is considered. Neutral pion decay is of historical importance since it is associated with the *axial anomaly*. The matrix element for  $\pi^0 \rightarrow \gamma\gamma$  decay (Fig. 17) is

$$\begin{aligned} \mathcal{T}(k_1, k_2) = & -2i \frac{\alpha_{em}}{\pi f_\pi} \epsilon_{\mu\nu\rho\sigma} \\ & \times \varepsilon^{\mu*}(k_1) \varepsilon^{\nu*}(k_2) k_{1\rho} k_{2\sigma} M(k_1, k_2), \end{aligned} \quad (45)$$

Since final photons are on-shell,  $k_i^2 = 0$ , and  $P^2 = (k_1 + k_2)^2 = 2 k_1 \cdot k_2 = m_\pi^2$ . Therefore the scalar function  $M(k_1, k_2)$  is only a function of the pion mass. The decay rate

$$\Gamma_{\pi^0 \rightarrow \gamma\gamma} = \left( \frac{\alpha_{em}}{\pi f_\pi} \right)^2 \frac{m_\pi^2}{16\pi} M(m_\pi^2), \quad (46)$$

is experimentally measured as  $\Gamma_{\pi^0 \rightarrow \gamma\gamma} = 7.74 \pm 0.56$  eV, which means

$$g_{\pi^0\gamma\gamma} \equiv M(m_\pi^2) = 0.504 \pm 0.019. \quad (47)$$

It has been shown in Ref. [28] that, in chiral limit, irrespective of the details of quark propagators, as long as the photon-quark vertices are properly dressed to conserve the electromagnetic current and the BS vertex function is properly normalized,  $g_{\pi^0\gamma\gamma}$  is analytically found to be 0.5. When the mass of the pion is taken into account, we find  $g_{\pi^0\gamma\gamma} = .43$  which is close to the experimental value.

A summary of the observables we calculated is given in Table 1. Error bars in experimental measurements are negligible unless indicated.

Observable	Calculated	Experimental
$m_\pi$ ( MeV)	148	139.6
$f_\pi$ ( MeV)	77.2	92.4
$\langle r_\pi^2 \rangle^{1/2}$ ( Fermi)	.65	.66
$g_{\pi^0\gamma\gamma}$	.43	.504
$m_\pi^*$ ( MeV)	1245	$1300 \pm 100$
$m_K$ ( MeV)	515	495
$f_K$ (MeV)	90.3	113
$\langle r_K^2 \rangle^{1/2}$ ( Fermi)	.54	.53
$f_K/f_\pi$	1.17	1.22
$r_K/r_\pi$	0.83	0.8

Table 1: Summary of results

## 5 CONCLUSION

In this work, we analyzed three aspects of the Dyson-Schwinger Bethe-Salpeter equation approach. We have shown that it is possible to dress the quark-gluon vertex beyond the simple  $\gamma^\mu$  form while maintaining the chiral limit condition. We have shown that an infrared finite gluon propagator can lead to confined quarks through generation of complex quark masses. It was found that, according to the model presented here, quarks can freely propagate only  $\approx 0.4$  Fermi which is in very good agreement with the hadronic bound state sizes. We have calculated all observables, including the pion form factor, using a Euclidean metric approach without relying on the analyticity properties of quark propagator functions  $A(p^2)$  and  $B(p^2)$ . It is found that the extrapolations associated with the usage of Euclidean metric are reliable up to  $1 \text{ GeV}^2$  for calculation of masses, and up to around  $.5\text{GeV}^2$  for the calculation of form factors.

## 6 ACKNOWLEDGMENTS

We gratefully acknowledge very useful and encouraging discussions with Dr. Craig Roberts. Dr. Conrad Burden is gratefully acknowledged for his input. This research was supported, in part by the U.S. National Science Foundation international Grant INT9021617. One of us(Ç. Ş.) has been supported by an Andrew Mellon Predoctoral Fellowship at the University of Pittsburgh, and by the DOE through grant No. DE-FG05-88ER40435. We

also acknowledge receipt of a grant of Pittsburgh Supercomputer Center computer time.

## A Numerical methods

Solutions of integral equations are performed by first discretizing the integrals

$$\int dq f(q) \longrightarrow \sum_{i=1}^n w_i f(q_i), \quad (48)$$

where  $w_i$  are integration weights for grid points  $q_i$ . In order to map the grid points and weights from interval  $(-1, 1)$  to  $(0, \infty)$  we use the arctangent mapping(Ref. [30, 31])

$$y(x) = R_{min} + \frac{R_d \tan(\frac{\pi}{4}(1+x))}{1 + \frac{R_d}{R_{max}-R_{min}} \tan(\frac{\pi}{4}(1+x))}, \quad (49)$$

where

$$R_d = \frac{R_{med} - R_{min}}{R_{max} - R_{med}}(R_{max} - R_{min}). \quad (50)$$

It follows that

$$y(-1) = R_{min}, \quad y(0) = R_{med}, \quad y(1) = R_{max}. \quad (51)$$

Therefore, one can safely control the range( $R_{min}, R_{max}$ ) and distribution( $R_{med}$ ) of grid points. With this discretization procedure, continuous integral equations are transformed into nonsingular matrix equations.

### A.1 Dyson-Schwinger Equation

The DS equation involves two unknown functions  $A, B$  which appear in two coupled equations(Eq. 3). After discretizing the associated integrals, one has the following matrix equations

$$\begin{aligned} B &= \mu I + G_1 F_1, \\ A &= I + G_2 F_2. \end{aligned} \quad (52)$$

$A, B, F_1$ , and  $F_2$  are  $n$  dimensional vectors where

$$\begin{aligned} F_1(i) &\equiv B(i)/(B(i)^2 q_i^2 + A(i)^2), \\ F_2(i) &\equiv A(i)/(B(i)^2 q_i^2 + A(i)^2), \end{aligned}$$

and  $G_1$  and  $G_2$  are  $n \times n$  matrices. Coupled equations(Eq. 52) are solved for  $A, B$  by forward iteration. An arbitrary initial guess for functions(vectors)  $A$  and  $B$  is entered on the right hand side and the resulting vectors are iteratively used for the same process until a stable solution is achieved. Grid points in momentum space have been chosen for momenta between  $R_{min} = 0$  MeV and  $R_{max} = 10^5 \sigma$  MeV where  $\sigma$  is the relevant momentum scale of the problem. The median of the grid point distribution was  $R_{med} = 5\sigma$  MeV. This uneven distribution of grid points ensures that the concentration of grid points for lower momenta, that is where the integrand is maximum, is higher. Due to the smooth nature of  $A$  and  $B$  functions only 40 grid points sufficed to find stable solutions. The number of iterations needed to find a stable result is around 20.

## A.2 Bethe-Salpeter Equation: Inverse Iteration Method

Here we outline the inverse iteration method originally developed in Refs. [30, 31].

The BS equation can be brought into the following form

$$[H_{M^2} - \alpha]\Phi = 0, \quad (53)$$

One starts with an arbitrary vector  $\chi^0$

$$\chi^0 = \sum_{i=1}^N c_i \Phi_i \quad (54)$$

where  $\Phi_i$ ,  $i = 1..N$ , satisfy

$$[H_{M^2} - \omega_i]\Phi_i = 0, \quad (55)$$

where  $\omega_i$ ,  $i = 1..N$  are eigenvalues of the  $H_{M^2}$  matrix. Next, an arbitrary first guess for  $\alpha$  is chosen. It should be emphasized that eigenvalues which are not equal to  $\alpha$  have no physical meaning, for they do not correspond to a solution of the BS equation(Eq. 53). In order to see if the initial guess  $\alpha$  corresponds to one of the eigenvalues  $\omega_i$ , we construct the operator

$$K = \frac{1}{H_{M^2} - \alpha}. \quad (56)$$

Operating  $K$  on state  $\chi^0$  n times produces

$$\chi^n = K^n \chi^0 = \sum_{i=1}^N \frac{c_i}{(\omega_i - \alpha)^n} \Phi_i. \quad (57)$$

When the number of iterations  $n$  is sufficiently large (usually around ten), the dominant contribution to  $\chi^n$  comes from the eigenvector  $\Phi_j$  whose eigenvalue  $\omega_j$  satisfies  $|\omega_j - \alpha| < |\omega_i - \alpha|$  for all  $i = 1..j-1, j+1..N$ . Therefore,

$$\begin{aligned}\chi^n &\approx \frac{c_j}{(\omega_j - \alpha)^n} \Phi_j, \\ \chi^{n+1} &\approx \frac{1}{\omega_j - \alpha} \chi^n.\end{aligned}\tag{58}$$

Using the eigenvector  $\chi^n$ , which is proportional to  $\Phi_j$ , one can also find eigenvalue  $\omega_j$  by

$$\omega_j = \frac{\chi^{n\dagger} H \chi^n}{\chi^{n\dagger} \chi^n}.\tag{59}$$

If  $\omega_j$  is close enough to  $\alpha$ , then one has a self consistent solution. This method has the benefit of directly singling out the eigenvalue closest to the initial guess, rather than finding the largest eigenvalue as in the case of straight forward iteration. There is only one matrix inversion involved. Distribution of the grid points in momentum space is done by the arctangent mapping, as in the solution of the Dyson-Schwinger equation. The typical number of momentum space grid points used in order to obtain stable solutions is around 40. For angular integrals, 20 grid points which are linearly distributed in interval  $(0, \pi)$  proved satisfactory.

### A.3 Confinement test

Since the test of confinement involves a highly oscillatory integral Eq. 26, we have used a large number, 30,000, of linearly distributed grid points. The upper limit of the momentum space integral, which is highly convergent, is  $400\sigma$ . These choices allow one to calculate the fourier transform (Eq. 26) confidently within the timeframe shown in Figures 5, 6, and 7.

## References

[\*] Research supported in part by the NSF.

- [1] C. D. Roberts and A. G. Williams, Prog. Part. Nucl. Phys. **33** (1994) 477.

- [2] Y. Nambu and G. Jona-Lasinio, Phys. Rev. **122**, 345 (1960); Phys. Rev. **124** (1961) 246.
- [3] H.J. Munczek, *Phys. Rev. D* **52** (1995) 4736.
- [4] A. Bender C. D. Roberts and L. V. Smekal, Phys. Lett. B **380** (1996) 7.
- [5] M. Buballa, S. Krewald, *Phys. Lett. B* **294** (1992) 19.
- [6] S.P.Klevansky, Rev. of Mod. Phys. **64** No.3 (1992) 649.
- [7] S. Klimt M. Lutz U. Vogl and W. Weise, Nucl. Phys. A **516**, (1990) 429; Nucl. Phys. A **516** (1990) 469.
- [8] L.S. Celenza, A. Pantziris, C.M. Shakin, J. Szweda, Phys. Rev. C **47** (1993) 2356; L. S. Celenza, C. M. Shakin, Wei-Dong Sun, Annals of Phys. **241** (1995) 1.
- [9] E. E. Salpeter, H. A. Bethe, Phys. Rev. **84** (1951) 1232.
- [10] S. Mandelstam, Proc. Roy. Soc. A **233** (1955) 248.
- [11] See Itzykson, C. and Zuber, J. *Quantum Field Theory*, (McGraw-Hill, Inc., 1980) for example.
- [12] R. Jackiw and K. Johnson, Phys. Rev. D **8** (1973) 2386.
- [13] R. Delbourgo and M. D. Scadron, J. Phys. G **5** (1979) 1621.
- [14] Marciano, W. and Pagels, H. Quantum Chromodynamics, Phys. Rep. **36** (1977) 137.
- [15] J. S. Ball and T.W. Chiu, Phys. Rev. D **22** (1980) 2542.
- [16] D. C. Curtis and M. R. Pennington, Phys. Rev. D **46**, (1992) 2663.
- [17] P. Jain and H.J. Munczek, Phys. Rev. D **46** (1992) 438.
- [18] P. Jain and H.J. Munczek, Phys. Rev. D **48** (1993) 5403.
- [19] J. Praschifka R. T. Cahill and C.D Roberts, Int. J. of Mod. Phys., **A4** (1989) 4929.

- [20] C.J. Burden, Lu Qian, C.D. Roberts, P.C. Tandy, nucl-th/9605027, (1996).
- [21] P.C. Tandy, Prog. Part. Nucl. Phys., Vol. **36** (1996) 97.
- [22] J. Gasser and H. Leutwyler, Physics Reports **87**, No 3 (1982) 77.
- [23] F. Gross and J. Milana, Phys. Rev. D **43** (1991) 2401; **45** (1992) 969; **50** (1994) 3332.
- [24] T. W. Allen C. J. Burden, Phys. Rev. D **53** (1996) 5842.
- [25] F. T. Hawes C. D. Roberts A. G. Williams, Phys. Rev D **49** (1994) 4683.
- [26] K. Kusaka and A. G. Williams, Phys. Rev. D **51** (1995) 7026.
- [27] F. T. Hawes K. Kusaka and A. G. Williams, hep-ph/9411238, (1994).
- [28] C. D. Roberts, Nucl. Phys. A **605** (1996) 475.
- [29] S.J. Stainsby R.T. Cahill, Phys. Lett. A 146 **9**, (1990) 467.
- [30] D. Heddle Y. R. Kwon F. Tabakin, Comp. Phys. Comm. **38** (1985) 71.
- [31] Y. R. Kwon F. Tabakin, Phys. Rev. C **18** (1978) 932.
- [32] L. S. Kisslinger and S.W. Wang, Nucl. Phys. B **399** (1993) 63.
- [33] S. R. Amendolia, *et al.*, Nucl. Phys. B **277** (1986) 168.
- [34] C. J. Bebek, *et al.*, Phys. Rev D **17**, No **7** (1978) 1693.
- [35] E. B. Dally, *et al.*, Phys. Rev. Lett. **45** (1980) 232.
- [36] S. R. Amendolia, *et al.*, Phys. Lett. B **178** (1986) 435.